ISSN (Print) 1226-1750
ISSN (Online) 2233-6656
**Journal of Magnetics** 23(2), 152-159 (2018) https://doi.org/10.4283/JMAG.2018.23.2.152

# Investigation of the Lift-off Effect on the Corrosion Detection Sensitivity of Three-axis MFL Technique

**T. Azizzadeh[1] and M. S. Safizadeh[2]***

[1]*Ph.D. Student, Department of Mechanical Engineering, Iran University of Science and Technology, Narmak 16887, Tehran, Iran*
[2]*Associate Professor, Department of Mechanical Engineering, Iran University of Science and Technology, Narmak 16887, Tehran, Iran*

(Received 21 October 2017, Received in final form 19 April 2018, Accepted 20 April 2018)

**Lift-off is considered as one of the most critical parameters that poses a major challenge in the appropriate application of magnetic flux leakage inspection technique. Sediments and welds are presented in the internal of all pipelines and cause lift-off. This paper investigates the influence of lift-off distances on the components of the three-axis MFL technique and, therefore, the lift-off effect on the corrosion detection sensitivity. COMSOL software is used to set up the 3D FEM modeling of three-axis MFL technique. In order to simulate internal pitting corrosion of oil and gas pipelines, two adjacent pits of different depths are modeled on the surface of a carbon steel plate. At a range of lift-off values, MFL responses from this defect geometry are computed and the relationships between the lift-off distances and obtained MFL signals are analyzed in detail. Finally, the validity of the simulation results is verified by experimental tests.**

**Keywords :** Three-axis MFL, Lift-off, 3D FEM, Pipeline inspection

## 1. Introduction

MFL is currently the most widely used and powerful technique for finding corrosion and other defects in ferromagnetic pipelines [1, 2]. In this technique, the wall of the pipeline is magnetized axially to the point of magnetic saturation through the incorporation of permanent magnets. Since the magnetic permeability of the ferromagnetic pipe is usually much greater than the surrounding free space, the ferromagnetic material has higher density of magnetic flux lines than free space. Therefore, a metal loss defect acts as a region of high magnetic reluctance causing an increased leakage field [3, 4]. This flux leakage can be measured by means of magnetic field sensors positioned as closely as possible to the surface of the pipe being tested [5]. The sensors can measure axial (Bx), radial (Bz) and circumferential (By) components of the magnetic flux leakage density. The shape and amplitude of the signals picked up by the sensors are used to characterization of the defects [6].

Lift-off is considered as one of the most critical parameters that influences the obtained MFL signals. The specific types of lift-off include sensor lift-off, magnetizer lift-off, or simultaneous sensor and magnetizer lift-off. The lift-off changes can be caused by welds, varying coating thickness or high-hardness sediments on the internal surface of the pipe. During the inspection process, changes in Lift-off distance can be resulted in inaccurate measurement of the amplitude of the MFL signals. Analysis of this inaccurate MFL signals could result in underestimating or missing defects [7-10]. Therefore, it is very important to investigate how the MFL signal varies with the changes in lift-off distance. The literature review indicates that most of the works on the lift-off influences on MFL signals have dealt with only the radial and axial components [11-15]. In particular, circumferential MFL component has largely been ignored. However, recent studies indicate that circumferential MFL component is an essential piece in the defect characterization puzzle [16-18]. In many studies, MFL signal treatment is investigated for a single defect. However, in real applications, multiple adjacent defects are most often encountered than single defects [19, 20]. Therefore, in this study, the defects were assumed to be closely-spaced pittings, as this is more similar to the real situation.

In this study, 3D FEM is adopted to investigate the influence of the lift-off distances on the three components of the MFL signals, as a result, the lift-off effect on the


*Corresponding author: Tel: +98-21-77240540
Fax: +98-21-77240488, e-mail: safizadeh@iust.ac.ir

corrosion detection sensitivity. The defect geometry consists of two adjacent pits that are vertically aligned to the applied magnetization direction. At a range of lift-off distances, the spatial distributions of axial (Bx), circumferential (By), and radial (Bz) MFL signals, for this defect geometry, are computed with the 3D FEM model. Also, the influences of the different lift-off distances on the MFL signals are investigated. Finally, the simulation results are verified by experimental measurements.

## 2. Simulation by 3D FEM

3D FEM is a powerful tool for the analysis of the magnetic circuit used in the MFL technique. It allows solving the non-linear equations governing the physical behavior of the system, and allows estimating the value of the magnetic field components at every point in the circuit. In this paper, COMSOL software is used to set up the 3D MFL model in the magnetostatic mode.

3D view of the MFL system together with the magnetic circuit arrangement is shown in Fig. 1(a). The magnetic circuit comprises magnets, couplings, yoke, and specimen. Figure 1(b) shows the saturation levels inside the specimen obtained from 3D model and how the magnetic field lines flow through the elements of the system. Magnetization is an important parameter of MFL technique for pipeline inspection [21].

As shown in Fig. 1(b), the flux lines originate at the north pole of the right magnet, pass through a ferromagnetic coupling, enter the plate wall, pass through the other ferromagnetic coupling, and then enter the south pole of the left magnet. Inside the ferromagnetic yoke, the flux lines flow from the left to the right, thus completing the magnetic circuit. Table 1 summarizes the dimensions, materials and magnetic properties of the magnetic circuit elements used in the simulation.

Adjacent pit defects with 10 mm diameter (2R) and different depths of 80 %t and 30 %t have been modeled on the specimen (t : plate thickness). The defects are located at the center area of the specimen and are vertically aligned to the applied magnetic field. Figure 2 schematically shows the pittings with edge-to-edge distance of 20 mm (4R).

To obtain the magnetic flux leakage data in the area of

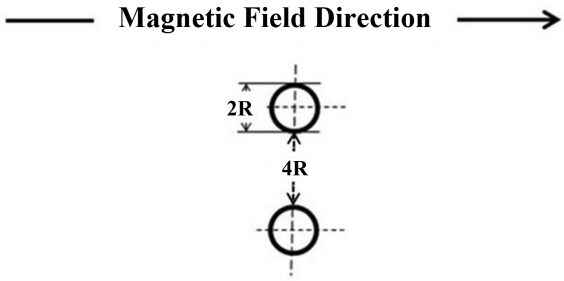


**Fig. 2.** Schematic representation of the circumferentially aligned adjacent pittings.

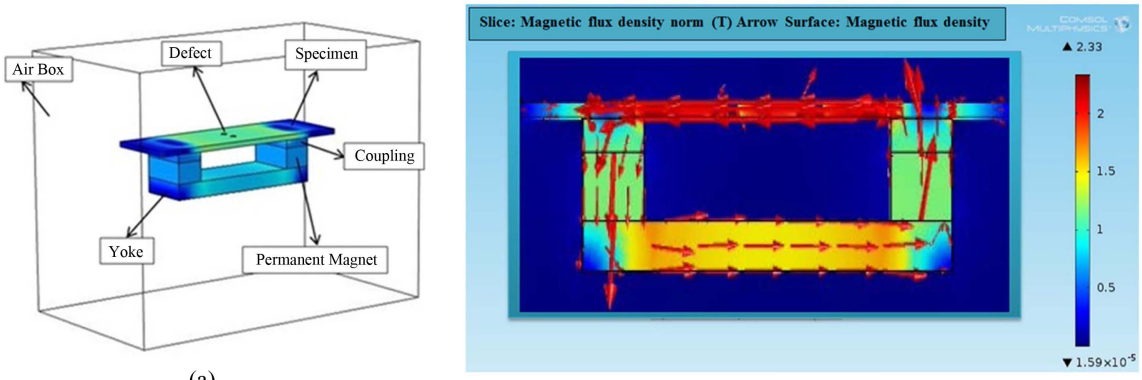


(a) (b)

**Fig. 1.** (Color online) (a) 3D view of the MFL system, (b) Magnetic flux behavior in the magnetic circuit.

**Table 1.** Dimensions and governing equations of the magnetic circuit elements.

| Component | Material | Length (mm) | Width (mm) | Depth (mm) | Governing equation |
|---|---|---|---|---|---|
| Plate | Steel X52 | 400 | 140 | 10 | $\|H\| = f(\|B\|)$ |
| Coupling | Steel X52 | 50 | 100 | 20 | $\|H\| = f(\|B\|)$ |
| Magnet | NdFeB | 50 | 100 | 40 | $B = \mu_0 H + \mu_0 M$ |
| Yoke | Steel X52 | 300 | 100 | 30 | $\|H\| = f(\|B\|)$ |
| Air Box | Air | 640 | 360 | 500 | $B = \mu_0 \mu_r H$ |

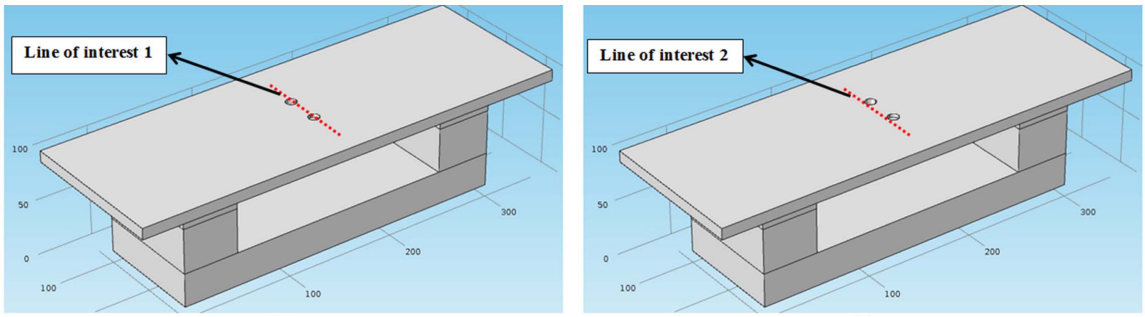


(a) (b)

**Fig. 3.** (Color online) The defined lines for obtaining: (a) Bx signal, (b) By and Bz signals.

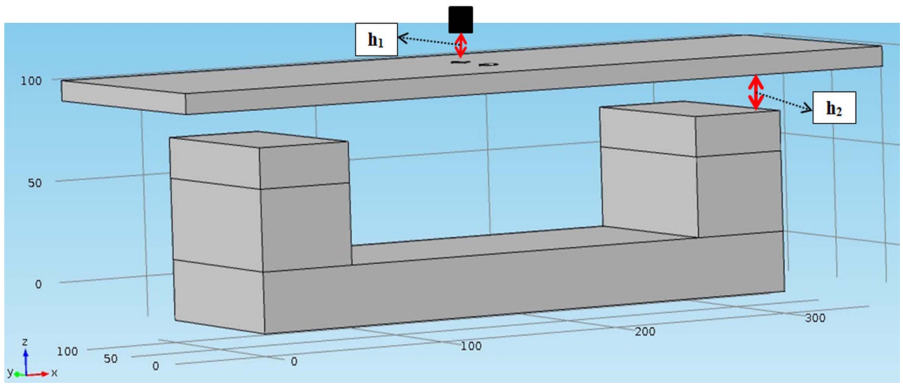


**Fig. 4.** (Color online) Schematic representation of the sensor lift-off ($h_1$) and the magnetizer lift-off ($h_2$).

the defects, a line at top of the specimen surface must be defined. Figure 3(a) shows the position of the line along which the axial (Bx) MFL signal is going to be calculated and then plotted. Figure 3(b) shows the position of the line along which the circumferential (By) and radial (Bz) MFL signals are going to be calculated and then plotted.

Figure 4 schematically shows the sensor lift-off ($h_1$) and the magnetizer lift-off ($h_2$). In particular, the influence of the lift-off distances on the components of the MFL signals is of interest.

### 2.1. The influence of sensor lift-off on MFL signals

While the magnetizer lift-off is zero, the sensor lift-off is set to be 1, 2, 4, 6, 8, and 10 mm respectively. For different values of the sensor lift-off, all three components of the MFL signals along the defined line-scans are calculated and then plotted. Figure 5 shows the influence of sensor lift-offs on the orthogonal components of the MFL signals for two adjacent pits.

It is evident from Figure 5 that the shape of the signals changes considerably with increasing the sensor lift-off. At low lift-off, all three MFL components exhibit a clear distinction of peak values and the two pittings can be easily distinguished while interacting with each other. At higher lift-off, sharp variations of the MFL signals are eliminated and all the peaks get diffused leading to low sensitivity. This phenomenon decreases the accuracy of the defect characterization although approximate defect dimensions can still be estimated.

Figure 6 shows the relation curve between sensor lift-offs and the amplitudes of three components of MFL signals for two adjacent pits. It is evident from Fig. 6 that the MFL peak amplitudes decrease significantly when the sensor lift-off is increased from 1 mm to 10 mm. Also, the curves indicate that low levels of sensor lift-off have a significant influence on the signal amplitudes. By analyzing the changes in axial and radial MFL peak amplitudes versus lift-off distances, it is evident that the deeper pitting has larger slopes. This suggests that the reduction in axial and radial MFL peak amplitudes due to lift-off is greater for deeper pitting. Also, the reduction in circumferential MFL peak amplitudes due to lift-off is greater for the shallower pitting.

Also, the relative amplitudes of the three MFL components for the two pittings at sensor lift-offs 1 mm and 10 mm are listed in Table 2. From Table 2, it is clear that axial MFL component is less sensitive to sensor lift-off in compared to the circumferential and radial MFL com-

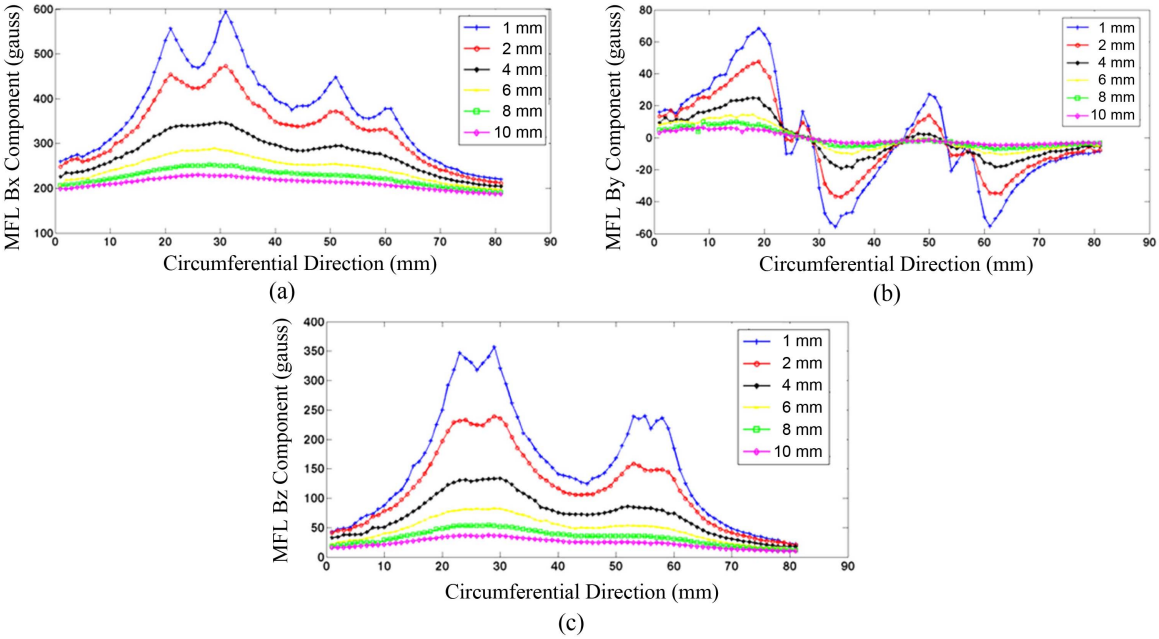


**Fig. 5.** (Color online) The influence of different sensor lift-offs on the: (a) axial, (b) circumferential, and (c) radial MFL signals.

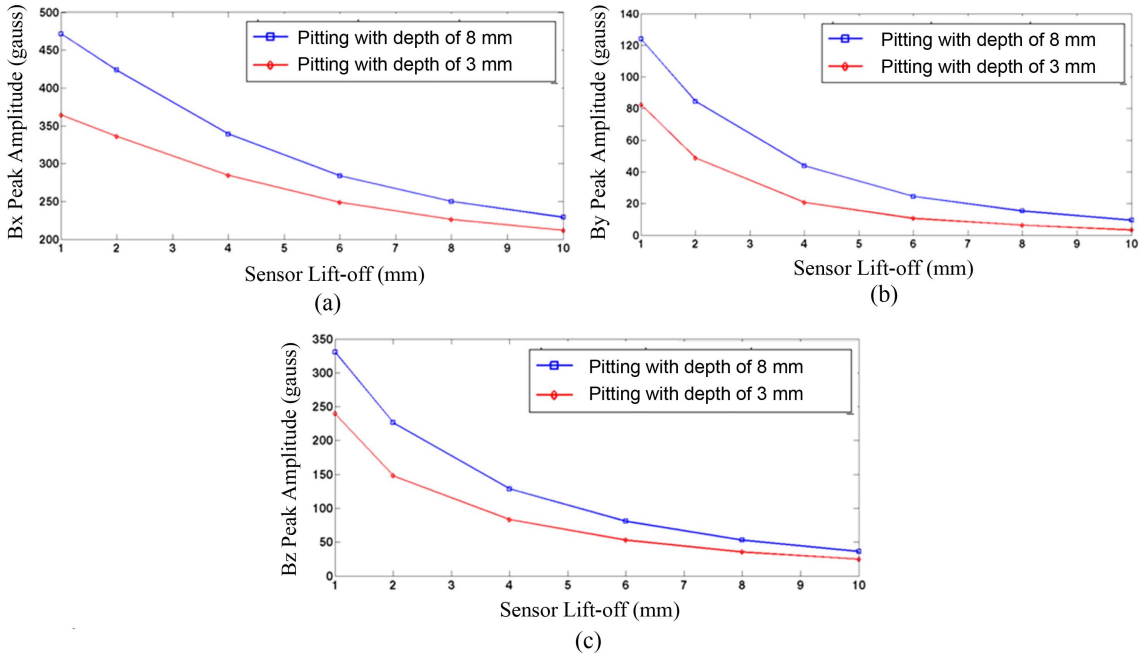


**Fig. 6.** (Color online) The relation curve between MFL amplitudes and sensor lift-offs: (a) axial, (b) circumferential, and (c) radial MFL signals.

**Table 2.** Relative amplitudes of MFL components for different sensor lift-offs.

| Pitting depth | $\frac{\max\lvert B_x\rvert_{h_1=1mm}}{\max\lvert B_x\rvert_{h_1=10mm}}$ | $\frac{\max\lvert B_y\rvert_{h_1=1mm}}{\max\lvert B_y\rvert_{h_1=10mm}}$ | $\frac{\max\lvert B_z\rvert_{h_1=1mm}}{\max\lvert B_z\rvert_{h_1=10mm}}$ |
|---|---|---|---|
| 8 mm | 2.06 | 13.23 | 9.67 |
| 3 mm | 1.72 | 24.8 | 9.18 |

ponents. Since axial MFL component has the lowest reduction of peak amplitude due to lift-off distances, its peak amplitude is a reliable cue for wall thickness measurement.

### 2.2. The influence of magnetizer lift-off on MFL signals

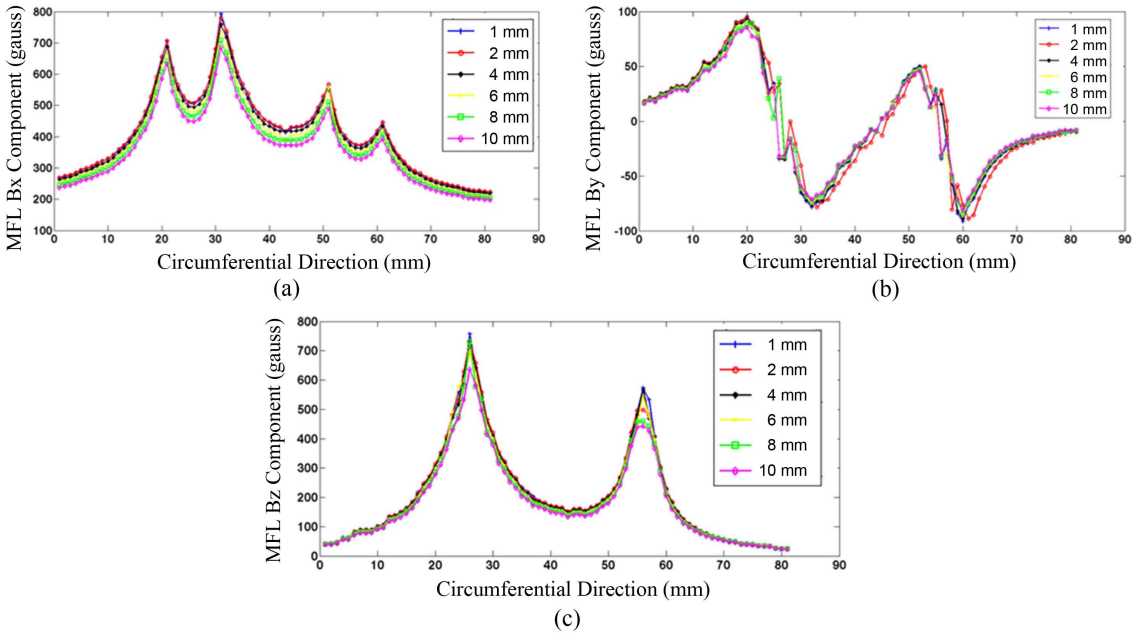


**Fig. 7.** (Color online) The influence of different magnetizer lift-offs on the: (a) axial, (b) circumferential, and (c) radial MFL signals.

To investigate the influence of magnetizer lift-off on MFL signals, various levels of the magnetizer lift-off (1, 2, 4, 6, 8, and 10 mm respectively) are considered while the sensor lift-off is zero. For different values of the magnetizer lift-off, all three components of the MFL signals along the defined line-scans are calculated and then plotted. Figure 7 shows the influence of magnetizer

**Table 3.** Relative amplitudes of MFL components for different magnetizer lift-offs.

| Pitting depth | $\frac{\max\lvert B_x\rvert_{h_2=1mm}}{\max\lvert B_x\rvert_{h_2=10mm}}$ | $\frac{\max\lvert B_y\rvert_{h_2=1mm}}{\max\lvert B_y\rvert_{h_2=10mm}}$ | $\frac{\max\lvert B_z\rvert_{h_2=1mm}}{\max\lvert B_z\rvert_{h_2=10mm}}$ |
|---|---|---|---|
| 8 mm | 1.14 | 1.11 | 1.18 |
| 3 mm | 1.13 | 1.2 | 1.13 |

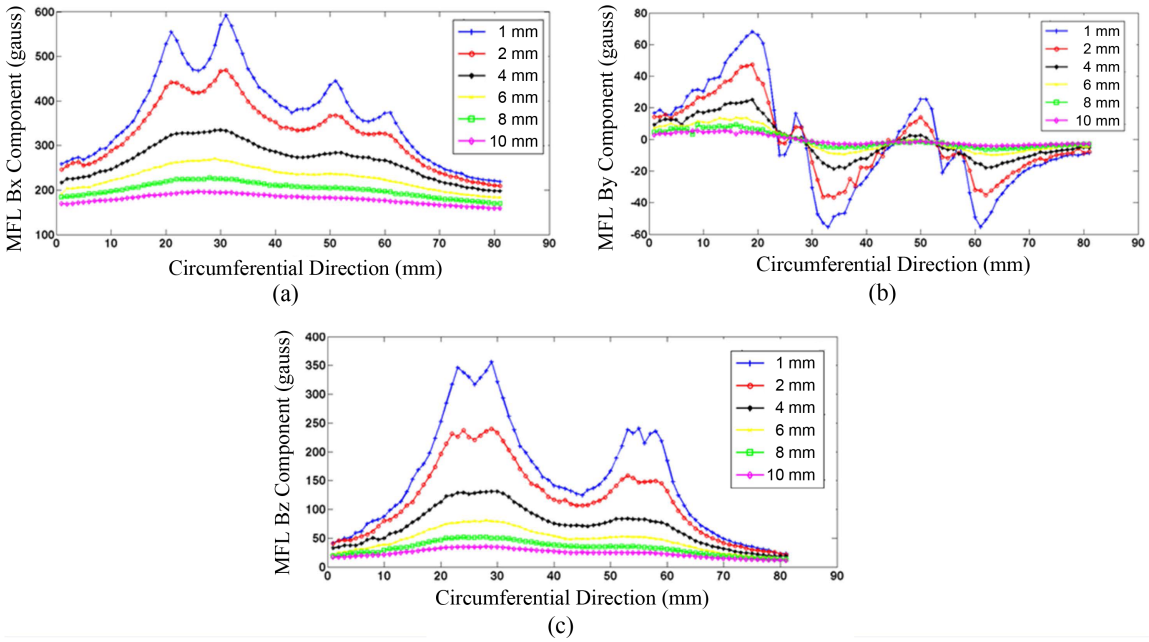


**Fig. 8.** (Color online) The influence of different magnetizer and sensor lift-offs on the: (a) axial, (b) circumferential, and (c) radial MFL signals.

**Table 4.** Relative amplitudes of MFL components for different magnetizer and sensor lift-offs.

| Pitting depth | $\frac{\max\|B_x\|_{h_1,h_2=1mm}}{\max\|B_x\|_{h_1,h_2=10mm}}$ | $\frac{\max\|B_y\|_{h_1,h_2=1mm}}{\max\|B_y\|_{h_1,h_2=10mm}}$ | $\frac{\max\|B_z\|_{h_1,h_2=1mm}}{\max\|B_z\|_{h_1,h_2=10mm}}$ |
|---|---|---|---|
| 8 mm | 2.4 | 14.57 | 9.96 |
| 3 mm | 2.01 | 27.74 | 9.64 |

lift-offs on the orthogonal components of the MFL signals for two adjacent pits.

Figure 7 shows the small reduction in MFL peak amplitudes and baseline MFL magnitudes with increasing magnetizer lift-off. Also in case of lower levels of lift-off, the influence of the magnetizer liftoff is not clearly pronounced for all three MFL components.

The relative amplitudes of the three MFL components for the two pittings at magnetizer lift-offs 1 mm and 10 mm are listed in Table 3. From Table 3, it is clear that magnetizer lift-off has less influence on the MFL signals in compared to sensor lift-off. This phenomenon will make it easier to design and manufacture MFL inspection equipment, because of no consideration to alignment and so on.

### 2.3. The influence of simultaneous sensor and magnetizer lift-off on MFL signals

To simulate various levels of simultaneous sensor and magnetizer lift-off, they are set to be 1, 2, 4, 6, 8, and 10 mm respectively. Figure 8 shows three components of the MFL signals while lift-off of sensor and magnetizer simultaneously changed. The simulation results demonstrate the significant reduction in peak amplitude and baseline MFL signals with increasing lift-off distance.

The relative amplitudes of the three MFL components for the two adjacent pittings at lift-offs 1 mm and 10 mm are listed in Table 4. The results indicate that circumferential MFL component is more sensitive to the simultaneous sensor and magnetizer lift-off in compared to the axial and radial MFL components.

### 2.4. The comparison of lift-off in all its forms

Figure 9 shows MFL signal comparison graphs at the same lift-off value of 2 mm in all its types. This Figure evidently indicates that sensor lift-off has a substantially greater influence on the MFL peak amplitude than magnetizer lift-off of the same value. Simultaneous lift-off of sensor and magnetizer produces the greatest reduction in the MFL peak amplitudes and baseline MFL magnitudes.

## 3. Experimental Validation

To verify the finite element analysis of lift-off influences, an experimental system was established [3], as shown in Figure 10. The geometrical parameters of the experimental system are the same as the ones as displayed in Table 1. The specimen under test is carbon steel plate of 10mm thickness, in which there are two blind-hole artificial

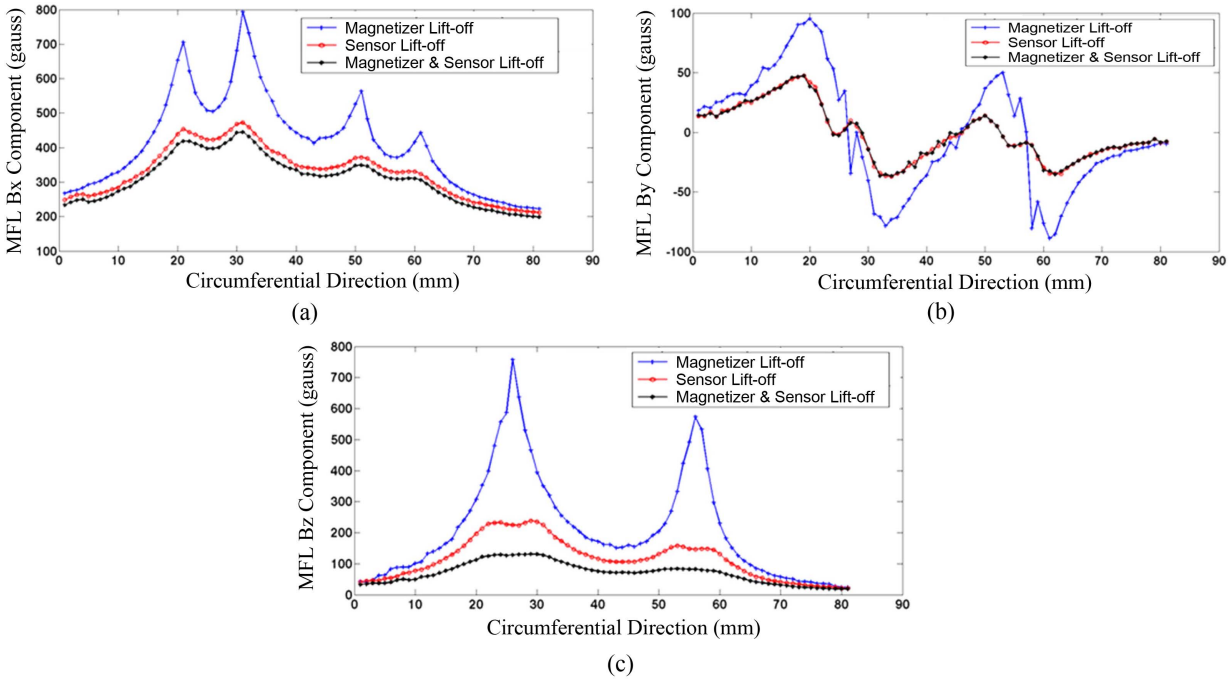


**Fig. 9.** (Color online) Comparison of the lift-off in all it forms: (a) axial, (b) circumferential, and (c) radial MFL signals.

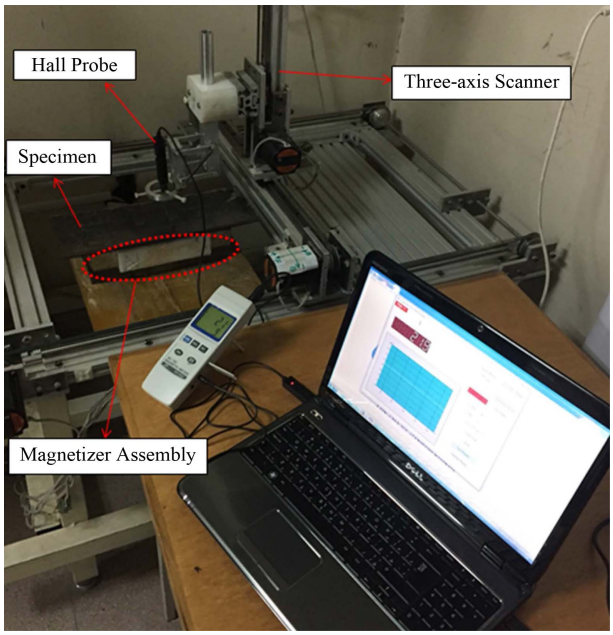


**Fig. 10.** (Color online) Experimental setup of the MFL measurements.

pittings with diameter of 10 mm and depths of 8 mm and 3 mm. The edge-to-edge distance of two pits is 20 mm and are vertically aligned to the applied magnetic field direction.

Hall sensor is used to perform a scan just along the line-scans being consistent with the simulation performed previously. The resolution of Hall sensor is better than search coil and also its range of linearity is higher than other kind of magnetic sensors [22]. The axial and circumferential components of the MFL signals are measured with Hall sensor. The lift-off distance between the plate surface and the sensor is maintained fixed (2 mm) since the sensor is moving by a three-axis scanner. The experimental test is carried out under magnetostatic conditions. Figure 11 respectively displays the axial and the circumferential leakage profiles picked up by the sensor together with the simulation results at 2mm sensor lift-off and zero magnetizer lift-off.

It can be seen from Figure 11 that there is good agreement between experimental and simulation values, both in magnitude and in shape. The numerical comparison of the experimental results and FEM results are indicated in Table 5.

## 4. Conclusion

In this work, a 3D finite element modeling of the three-axis MFL technique was designed in order to investigate the influence of lift-off distances on the components of the MFL signals and corrosion detection sensitivity. Two adjacent pitting defects of different depths on a plate have been modeled. At a range of lift-off distances, the magnetic flux leakage responses from this defect geometry have been obtained. Based on these studies the following conclusions can be drawn:

1) Lift-off in all its types causes a reduction in the peak

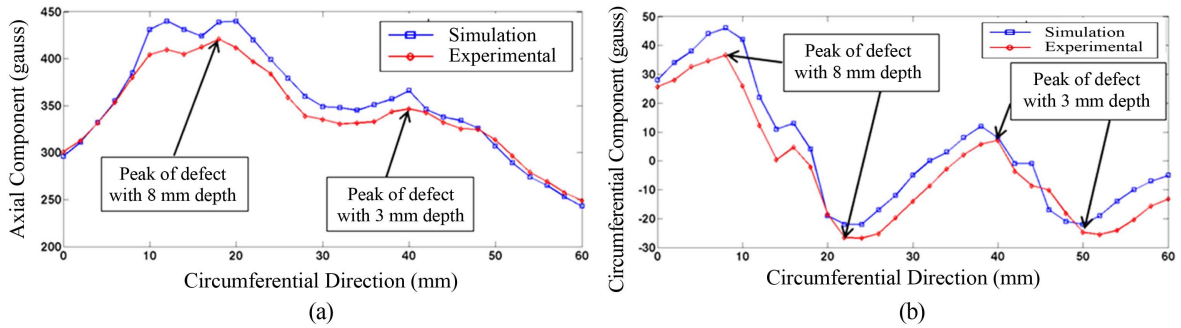


**Fig. 11.** (Color online) Comparison between experimental and FEM results: (a) axial, (b) circumferential MFL component.

**Table 5.** Numerical Comparison between experiments and FEM.

| MFL component | Pitting diameter (mm) | Pitting depth (mm) | Experiment MFL peak value (gauss) | FEM MFL peak value (gauss) | Experiment MFL peak-to-peak value (gauss) | FEM MFL peak-to-peak value (gauss) | Relative Error (%) |
|---|---|---|---|---|---|---|---|
| Axial MFL | 10 | 8 | 420 | 440 | - | - | 4.5 |
| Axial MFL | 10 | 3 | 340 | 360 | - | - | 5.5 |
| Circumferential MFL | 10 | 8 | - | - | 63 | 68 | 7.3 |
| Circumferential MFL | 10 | 3 | - | - | 32 | 34 | 5.8 |

and baseline MFL amplitudes.

2) The magnetizer lift-off has very small influence on the peak and baseline MFL amplitudes.

3) Simultaneous sensor and magnetizer lift-off causes the greatest reduction in peak MFL amplitudes.

4) Sensor lift-off produces approximately the same value of signal attenuation as simultaneous sensor and magnetizer lift-off.

5) Very low levels of lift-off (sensor lift-off or simultaneous sensor and magnetizer lift-off) can cause significant reductions in the measured MFL amplitudes.

6) The axial MFL component is less sensitive to lift-off distances in compared to the circumferential and radial MFL components.

7) The influence of lift-off on the circumferential MFL component is more pronounced than the axial and radial MFL components.

8) In the case of adjacent pittings vertically aligned to the applied magnetic field, width estimation of defects is difficult. This dimension can be accurately estimated using circumferential MFL component at low lift-off.

9) In the case of adjacent pittings and at higher lift-off, sharp variations of the MFL signals are eliminated and all the peaks get diffused leading to low sensitivity.

10) The reductions in the MFL signal amplitudes have the potential to cause shallower defects to be missed and deeper defects to be severely undersized. Both cases are unfavorable and can influence the reliability of the MFL signals.

Finally, the validity of the simulation results was verified by experimental tests in the laboratory facilities. At 2 mm sensor lift-off and zero magnetizer lift-off, a comparison between simulation and experimental results was performed. The relative error between the simulation and experimental results was approximately 7 %.

## References

[1] S. H. Choi, H. R. Yoo, D. K. Kim, D. J. Park, Y. W. Rho, K. Seo, G. S. Park, D. H. Choi, and S. J. Song, J. Magn. **15**, 199 (2010).
[2] P. Ramuhalli, L. Udpa, and S. S. Udpa, J. Appl. Phys. **93**, (2003).
[3] T. Azizzadeh and M. S. Safizadeh, NDT.net (2017).
[4] X. B. Li, X. Li, and L. Chen, J. Mech. Sci. Technol. **23**, 1 (2009).
[5] R. Brandstrom, U.S. Patent 7,804,295, 28 (2010).
[6] F. Ji, C. Wang, X. Zuo, S. Hou, and S. Liang, Insight. **49**, 9 (2007).
[7] American Society for Nondestructive Testing, Nondestructive Testing Handbook, Second Edition, The American Society of Nondestructive Testing (1986).
[8] J. H. Tiratsoo, Gulf Publishing Companyand Scientific Surveys Ltd. Houston, TX (1991).
[9] J. B. Nestleroth, update to Gas Research Institute Report GRI-91/0367, to be published.
[10] F. Valentine, OGJ. (2000).
[11] M. Katoh, N. Masumoto, K. Nishio, and T. Yamaguchi, NDT & E Int. **36**, 7 (2003).
[12] H. Zuoying, Q. Peiwen, and C. Liang, NDT & E Int. **39**, 61 (2006).
[13] R. Christen, A. Bergamini, and M. Motavalli, NDT & E Int. **42**, 22 (2009).
[14] J. A. Parra-Raad and S. Roa-Prada, J. Nondestruct. Eval. **35**, 14 (2016).
[15] V. Suresh and A. Abudhahir, Measurement Sci. Rev. **16**, 1 (2016).
[16] Y. Li, J. Wilson, and G. Tian, NDT & E Int. **40**, 2 (2007).
[17] S. M. Dutta, F. H. Ghorbel, and R. K. Stanley, IEEE Trans. Magn. **45**, 4 (2009).
[18] G. Kopp and H. Willems, NDT & E Int. **55**, 75 (2013).
[19] Y. Gunaltun, OGJ. **97**, 28 (1999).
[20] J. H. Kim, M. H. Kim, and D. H. Choi, J. Magn. **18**, 2 (2013).
[21] G. S. Park, P. W. Jung, and Y. W. Rho, J. Magn. **6**, 31 (2001).
[22] D. G. Park, M. B. Kishore, J. Y. Kim, L. J. Jacobs, and D. H. Lee, J. Magn. **21**, 57 (2016).